Electronic Supporting Information for

Zeolite analogs based on oxysulfidometalate supertetrahedral clusters via Coulombic interactions

Ming-Bu Luo,[a] Jun-Li chen,[a] Shan-Lin Huang,[a] Xuechou Zhou,[d] Er-Xia Chen*[a,b,c] and Qipu Lin*[a,c]

[a]*State Key Laboratory of Structural Chemistry, Fujian Institute of Research on the Structure of Matter, Chinese Academy of Sciences, Fuzhou, Fujian 350002, China*

[b]*Fujian Science & Technology Innovation Laboratory for Optoelectronic Information of China, Fuzhou, Fujian 350108, China*

[c]*State Key Laboratory of Photocatalysis on Energy and Environment, Fuzhou University, Fuzhou, 350116, China*

[d]*School of Life Sciences, Fujian Agriculture and Forestry University, Fuzhou, Fujian 350000, China*

*Corresponding Author: Email: exchen@fjirsm.ac.cn; linqipu@fjirsm.ac.cn

Table of Contents

Section S1: General Methods

Chemicals: *n*-Butyltin trichloride ($^{n}BuSnCl_3$, 98%), indium acetate hydrate (In(OAc)$_3$·6H$_2$O, 99.9%), zinc acetate dihydrate (Zn(oac)$_2$·2H$_2$O, 99.9%), lanthanum nitrate hexahydrate (La(NO$_3$)$_3$·6H$_2$O, 99%), stannous chloride dihydrate (SnCl$_2$·2H$_2$O, 98%), thiourea ((NH$_2$)$_2$CS, 99%), triethylene glycol (TEG, 98%), *N*-methyl-2-pyrrolidone (NMP, 98%), tetramethylguanidine (TMG, 99%), dibenzylamine (DBA, 99%), 1-methylpiperidine (MPI, 98%), 2-amino-1-butanol (98%) were acquired from Aladdin Chemical Reagent Shanghai. All chemicals were used as supplied without further purification.

Instrumentation: Energy dispersive spectroscopy (EDS) analysis was performed on scanning electron microscope (SEM) coupled with Oxford INCA system. Elemental analysis (EA) data was collected on a Vario EL-Cube instrument. Inductively coupled plasma optical emission spectroscopy (ICP–OES) was carried out an Ultima-2 spectrometer device. The powder X-ray diffraction (PXRD) data of the crystals were collected on a Rigaku Mini Flex II diffractometer using Cu Kα radiation (λ = 1.54056 Å) operated at 30 kV and 10 mA under ambient conditions. The solid-state ultraviolet visible (UV–Vis) diffuse reflection spectroscopy (DRS) were recorded at room temperature with BaSO$_4$ as a reference substance (100% reflectance) on a PerkinElmer Lamda-950 UV spectrophotometer and scanned at 250–800 nm. Thermo gravimetric analysis (TGA) was performed on a Mettler Toledo TGA/SDTA 851e analyzer in air atmosphere with a heating rate of 10 °C min^{-1} under N$_2$ flow from room temperature to 800 °C. Fourier transform infrared (FT–IR) spectra were acquired using KBr pellets on a Nicolet Magna 750 FT–IR spectrometer between 400–4000 cm^{-1} in attenuated total reflection. Electrospray ionization-mass (ESI-MS) measurements were performed on an Impact II UHR-TOF (Bruker).

Crystallographic Characterization: The single crystal X-ray diffraction measurement was performed on a ROD, Synergy Custom system, HyPix diffractometer with micro-focus metaljet Kα (λ = 1.34050 Å) radiation at 100 K. The structures were solved by direct method and refined by full-matrix least-squares on F^2 using the olex2.[1] All the

non-hydrogen atoms are refined anisotropically. Contributions to scattering due to disordered solvent molecules were removed using the SQUEEZE routine of PLATON.[2] The structures were then refined again using the data generated.

Impedance analysis: The samples were dried at 60 °C in oven overnight and then put into a home-made mold with a diameter of 0.4 cm to get circular pellets, whose thickness was measured by a micrometer screw. Two sides of the pellets were smeared by silver colloid, and further connected by copper wires, respectively. The proton conductivities were evaluated by using a Zahner (IM6) electrochemical impedance spectrometer, over a frequency range from 100 mHz to 10 MHz, under varying temperatures (room temperature to 50 °C) and different relative humidity (75% to 98% RH). The proton conductivity was calculated by using the following equation

$$\sigma = \frac{l}{SR}$$

Where σ is the conductivity (S cm^{-1}), l is the thickness (cm) of the pellet, S is the cross-sectional area (cm^2) of the pellet and R is the bulk resistance (Ω). The activation energy (E_a) was calculated from the following equation

$$ln\ \sigma_T = ln\ \sigma_0 - \frac{E_a}{RT}$$

Where σ is the conductivity (S cm^{-1}), K is the Boltzmann constant (eV K^{-1}) and T is the temperature (K).

Section S2: Synthetic Procedures

Synthesis of T3-MEP [Sn$_{10}$S$_{20}$O$_4$]·1.5LaCl$_3$·[C$_5$H$_9$NOH]$_8$·[C$_5$H$_9$NO]$_2$·[C$_6$H$_{14}$O$_4$]$_2$

^{n}BuSnCl$_3$ (0.1 mL), SnCl$_2$·2H$_2$O (0.35 mmol, 79.0 mg), La(NO$_3$)$_3$·6H$_2$O (0.30 mmol, 129.9 mg), thiourea (2 mmol, 152.2 mg), NMP (3.0 mL), TEG (2.0 mL) were mixed in a 23-mL Teflon-lined stainless autoclave and stirred for 10 min. Then the vessel was sealed and heated at 120 °C for 8 days. Colorless octadecahedron-shaped crystals (yield: 62 mg, ca. 18.35% base on ^{n}BuSnCl$_3$ and SnCl$_2$·2H$_2$O) with pure phase were obtained after 3 days in room temperature and washed with ethanol for several times. Experimental EA data: C 20.15%, H 3.3%, N 3.89%, S 16.66%; calculated EA data: C 20.9%, H 3.53%, N 3.93%, S 18.01%. Experimental ICP data: Sn 33.65%, La 5.47%; calculated ICP data: Sn 33.34%, La 5.85%; IR: v (cm^{-1}) = 2925(w), 2868(w), 1643(s), 1512(m), 1461(w), 1410(w), 1311(w), 1260(w), 1227(w), 1175(w), 1124(w), 1069(w), 989(w), 932(w), 895(w), 750(w), 666(w), 559(m), 465(w).

Synthesis of T4-MTN [Sn$_4$In$_{12}$Zn$_4$S$_{31}$O$_4$][C$_5$H$_{14}$N$_2$O]$_4$·[C$_5$H$_{14}$N$_3$]$_2$

^{n}BuSnCl$_3$ (10 μL), In(OAc)$_3$·6H$_2$O (0.20 mmol, 80.0 mg), Zn(OAc)$_2$·2H$_2$O (0.10 mmol, 22.0 mg), thiourea (3 mmol, 228 mg), TMG (1.25 mL), DBA (2.5 mL), H$_2$O (1 mL) were mixed in a 23-mL Teflon-lined stainless autoclave and stirred for 20 min. Then the vessel was sealed and heated at 120 °C for 7 days. Colorless or pale-yellow octahedral crystals (yield: 12 mg, ca. 20.63% base on ^{n}BuSnCl$_3$) with pure phase were obtained by filtration after being washed with acetone and water for several times. Experimental EA data: C 9.95%, H 2.91%, N 4.81%, S 25.14%; calculated EA data: C 10.83%, H 2.17%, N 5.06%, S 25.63%. Experimental ICP data: Sn 10.46%, In 30.05%, Zn 4.68%; calculated ICP date: Sn 12.25%, In 35.54%, Zn 6.74%. IR: v (cm^{-1}) = 3579(w), 3524(w), 3449(w), 3378(w), 2957(w), 2912(w), 2846(w), 2761(w), 1617(m), 1457(s), 1296(w), 1247(w), 1171(w), 1140(w), 1065(w), 1021(m), 815(m), 669(m), 503(s).

Synthesis of T4-DIA [Sn$_4$In$_{12}$Zn$_4$S$_{31}$O$_4$][C$_6$H$_{14}$N]$_8$·[C$_4$H$_{13}$NO]

^{n}BuSnCl$_3$ (10 μL), In(OAc)$_3$·6H$_2$O (0.20 mmol, 80.0 mg), Zn(OAc)$_2$·2H$_2$O (0.10 mmol, 22.0 mg), thiourea (3 mmol, 228 mg), MPI (2 mL), 2-amino-1-butanol (1 mL), H$_2$O (0.5 mL), were mixed in a 23-mL Teflon-lined stainless autoclave and stirred for 20 min.

Then the vessel was sealed and heated at 120 °C for 7 days. Colorless or pale-yellow octahedral crystals (yield: 34 mg, ca. 55.77% base on ^{n}BuSnCl$_3$) with pure phase were obtained by filtration after being washed with ethanol for several times. Experimental EA data: C 16.59%, H 3.23%, N 2.655%, S 25.4%; calculated EA data: C 15.35%, H 2.85%, N 3.1%, S 24.4%. Experimental ICP data: Sn 10.4%, In 26.18%, Zn 4.58%; calculated ICP data: Sn 11.68%, In 33.9%; Zn 6.43%. IR: v (cm^{-1}) = 2952(s), 2861(m), 2676(w), 2550(w), 2510(w), 2470(w), 1678(m), 1592(m), 1457(s), 1371(m), 1311(w), 1241(w), 1171(w), 1140(w), 1105(w), 1055(m), 1026(w), 994(w), 966(w), 943(w), 850(w), 689(w), 661(w), 592(w), 541(w), 502(w), 453(w).

Synthesis of T4-LON [Sn$_4$In$_{12}$Zn$_4$S$_{31}$O$_4$][C$_5$H$_{14}$N$_2$O]$_5$

^{n}BuSnCl$_3$ (10μL), In(OAc)$_3$·6H$_2$O (0.20 mmol, 80.0 mg), Zn(OAc)$_2$·2H$_2$O (0.10 mmol, 22.0 mg), thiourea (3 mmol, 228 mg), TMG (1.25 mL), H$_2$O (0.5 mL), were mixed in a 23-mL Teflon-lined stainless autoclave and stirred for 20 min. Then the vessel was sealed and heated at 120 °C for 7 days. Colorless or pale-yellow hexagonal prism crystals (yield: 23 mg, ca. 40.74% base on ^{n}BuSnCl$_3$) with pure phase were obtained by filtration after being washed with acetone and water for several times. Experimental EA data: C 8.82%, H 2.7%, N 3.24%, S 26.76%; calculated EA data: C 7.97%, H 1.86%, N 3.72%, S 26.36%. Experimental ICP data: Sn 11.35%, In 35.48%, Zn 5.99%. calculated ICP data: Sn 12.62%, In 36.61%, Zn 6.95%. IR: v (cm^{-1}) = 3364 (w), 2952(w), 2912(w), 2847(w), 2747(w), 2405(w), 1652(s), 1457(s), 1381(m), 1246(w), 1171(w), 1140(w), 1076(w), 1045(w), 1015(m), 879(w), 815(m), 694(w), 664(w), 589(w), 504(w).

Section S3: Electrospray Ionization Mass Spectrometry (ESI–MS)
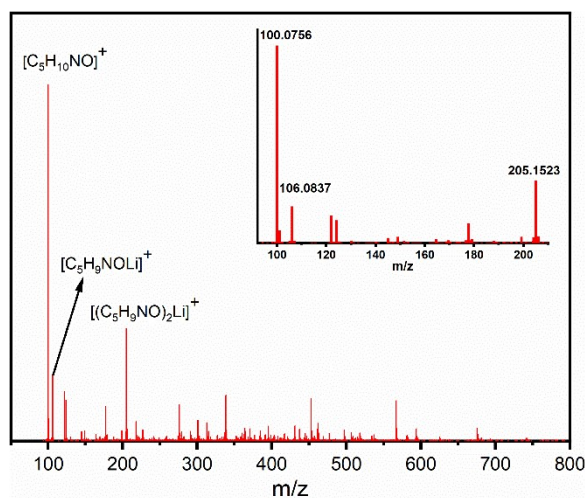
Fig. S1 The positive-mode ESI-MS spectrum of T3-MEP in CH_3OH with addition of LiCl. The main peak at 100.0756 could be assignable to species of protonated *N*-methyl-2-pyrrolidone (H^+NMP, $[C_5H_{10}NO]^+$). The minor peaks at 106.0837 and 205.1523 could be assignable to species of $[C_5H_9NOLi]^+$) and $[(C_5H_9NO)_2Li]^+$, respectively.
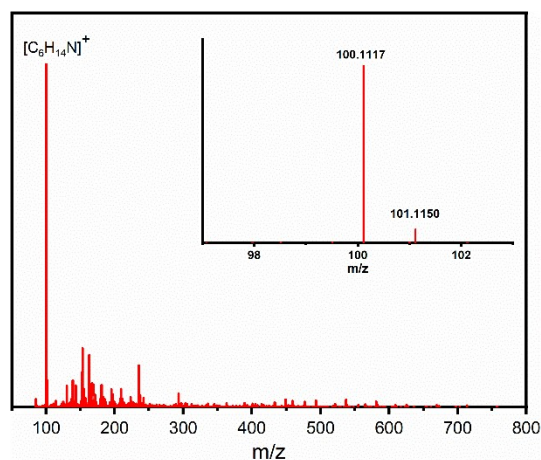
Fig. S2 The positive-mode ESI-MS spectrum of T4-DIA in CH_3OH. The main peak at 100.1117 could be assignable to species of protonated 1-methylpiperidine (H^+MPI, $[C_6H_{14}N]^+$).
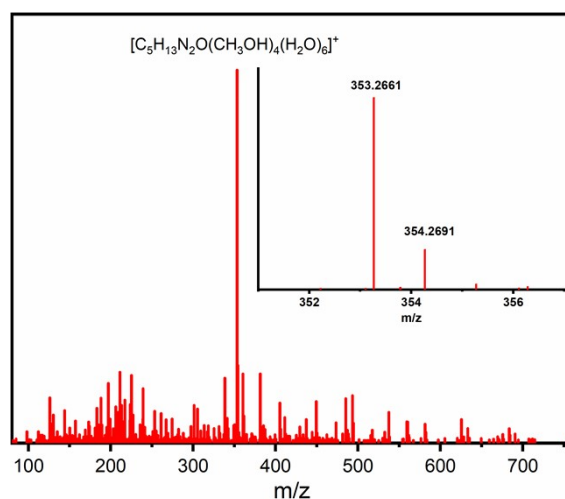
Fig. S3 The positive-mode ESI-MS spectrum of T4-LON in CH_3OH. The main peak at 353.2661 could be assignable to species of protonated tetramethylurea (H^+TMU, where the TMU is derived from the hydrolysis of TMG used) coupled with CH_3OH and H_2O (i.e.,$[C_5H_{13}N_2O(CH_3OH)_4(H_2O)_6]^+$).
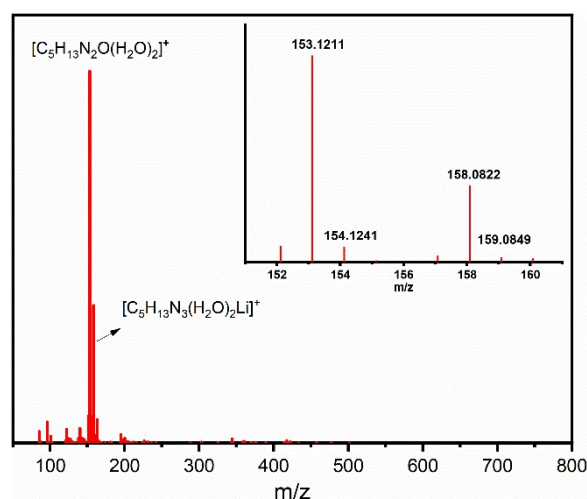
Fig. S4 The positive-mode ESI-MS spectrum of T4-MTN in CH_3OH with addition of LiCl. The main peak at 153.1211 could be assignable to species of protonated tetramethylurea (H^+TMU, where the TMU is derived from the hydrolysis of TMG used) coupled with H_2O (i.e., $[C_5H_{13}N_2O(H_2O)_2]^+$). The minor peak at 158.0822 could be assignable to species of protonated tetramethylguanidine (H^+TMG) with Li^+ and H_2O (i.e., $[C_5H_{13}N_3(H_2O)_2Li]^+$).

Section S4: Crystallographic Data

Table S1 Lattice parameters of tin-based oxychalcogenide clusters by SCXRD

Compound Name	T3-MEP	T4-DIA	T4-LON	T4-MTN
a/ Å	50.5840(2)	31.1300(16)	41.1511(8)	80.4375(6)
b/ Å	50.5840(2)	31.1300(16)	41.1511(8)	80.4375(6)
c/ Å	50.5840(2)	31.1300(16)	36.6354(9)	80.4375(6)
α/°	90	90	90	90
β/°	90	90	90	90
γ/°	90	90	120	90
Volume /Å^3	129431.4 (9)	30167(3)	53727(2)	520446(7)

Table S2 Calculation of void ratio and surface area of tin-based oxychalcogenide clusters by PLATON and Materials Studio

Compound Name	T3-MEP	T4-DIA	T4-LON	T4-MTN
Void ratio/ %	73	66.4	60.7	64.8
surface area /$m^2 \cdot g^{-1}$	1615.77	1409.85	1466.59	1491.98

Table S3 Crystallographic data of tin-based oxychalcogenide clusters

Compounds	T3-MEP	T4-DIA
CCDC#	2241505	2241506
Empirical formula	$O_{92}S_{460}Sn_{230}$	$In_{12}O_4S_{31}Sn_4Zn_4$
Formula weight	43518.3	3171.94
Temperature/K	100.01(10)	100.00(10)
Crystal system	cubic	cubic
Space group	Pm-3n	Fd-3m
a/Å	50.5840(2)	31.1300(16)
b/Å	50.5840(2)	31.1300(16)
c/Å	50.5840(2)	31.1300(16)
$\alpha/°$	90	90
$\beta/°$	90	90
$\gamma/°$	90	90
Volume/Å^3	129431.4(15)	30167(5)
Z	2	8
ρ_{calc}g/cm^3	1.117	1.397
μ/mm^{-1}	13.945	16.492
F(000)	39192	11488
Crystal size/mm^3	0.08 × 0.08 × 0.08	0.2 × 0.2 × 0.2
Radiation	GaKα (λ = 1.3405)	GaKα (λ = 1.3405)
2Θ range for data collection/°	4.802 to 104.98	6.982 to 67.854
Index ranges	-28 ≤ h ≤ 59, -27 ≤ k ≤ 45, -54 ≤ l ≤ 43	-25 ≤ h ≤ 25, -20 ≤ k ≤ 25, -19 ≤ l ≤ 25
Reflections collected	161760	7324
Independent reflections	19367 [R_{int} = 0.1383, R_{sigma} = 0.0572]	472 [R_{int} = 0.0795, R_{sigma} = 0.0180]
Data/restraints/parameters	19367/13/322	472/0/33
Goodness-of-fit on F^2	1.09	1.087
Final R indexes [I>=2σ (I)]	R_1 = 0.1021, wR_2 = 0.2859	R_1 = 0.0792, wR_2 = 0.2192
Final R indexes [all data]	R_1 = 0.1104, wR_2 = 0.2922	R_1 = 0.1104, wR_2 = 0.2728
Largest diff. peak/hole / e Å^{-3}	1.33/-1.95	0.58/-0.32

Compounds	T4-LON	T4-MTN
CCDC#	2241507	2241508
Empirical formula	$In_{12}O_4S_{31}Sn_4Zn_4$	$In_{12}O_4S_{31}Sn_4Zn_4$
Formula weight	3171.94	3171.94
Temperature/K	293(2)	293(2)
Crystal system	hexagonal	cubic
Space group	$P6_3/m$	Fd-3m
a/Å	41.2494(6)	80.4375(6)
b/Å	41.2494(6)	80.4375(6)
c/Å	36.6629(7)	80.4375(6)
α/°	90	90
β/°	90	90
γ/°	120	90
Volume/Å^3	54024.7(19)	520446(12)
Z	16	136
ρ_{calc}g/cm^3	1.56	1.376
μ/mm^{-1}	18.418	16.251
F(000)	22976	195296
Crystal size/mm^3	0.3 × 0.1 × 0.1	0.2 × 0.2 × 0.15
Radiation	GaKα (λ = 1.3405)	GaKα (λ = 1.3405)
2Θ range for data collection/°	17.738 to 112.528	3.82 to 74.988
Index ranges	$-50 \leq h \leq 51$, $-35 \leq k \leq 47$, $-31 \leq l \leq 45$	$-73 \leq h \leq 68$, $-73 \leq k \leq 60$, $-70 \leq l \leq 59$
Reflections collected	134605	151443
Independent reflections	35436 [R_{int} = 0.1210, R_{sigma} = 0.0721]	9210 [R_{int} = 0.0937, R_{sigma} = 0.0287]
Data/restraints/parameters	35436/0/661	9210/53/408
Goodness-of-fit on F^2	1.053	1.179
Final R indexes [I>=2σ (I)]	R_1 = 0.0586, wR_2 = 0.1728	R_1 = 0.0870, wR_2 = 0.2608
Final R indexes [all data]	R_1 = 0.0979, wR_2 = 0.1916	R_1 = 0.1070, wR_2 = 0.2888
Largest diff. peak/hole / e Å^{-3}	1.52/-0.92	0.76/-0.63

T3-MEP   T4-DIA

T4-LON   T4-MTN
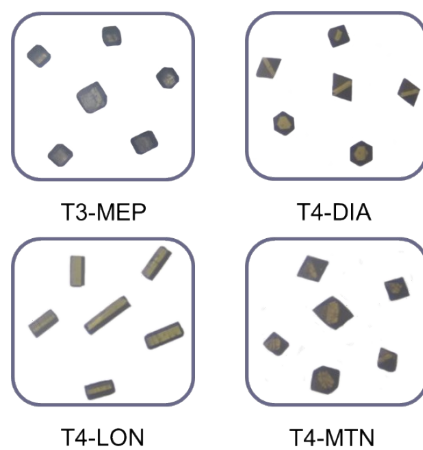
Fig. S5 The photographs of the crystals
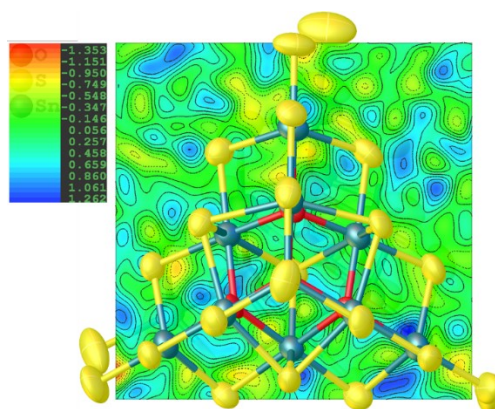
Fig. S6 The the electron density difference map between two clusters in T3-MEP. The blue contours represent as H^+NMP.
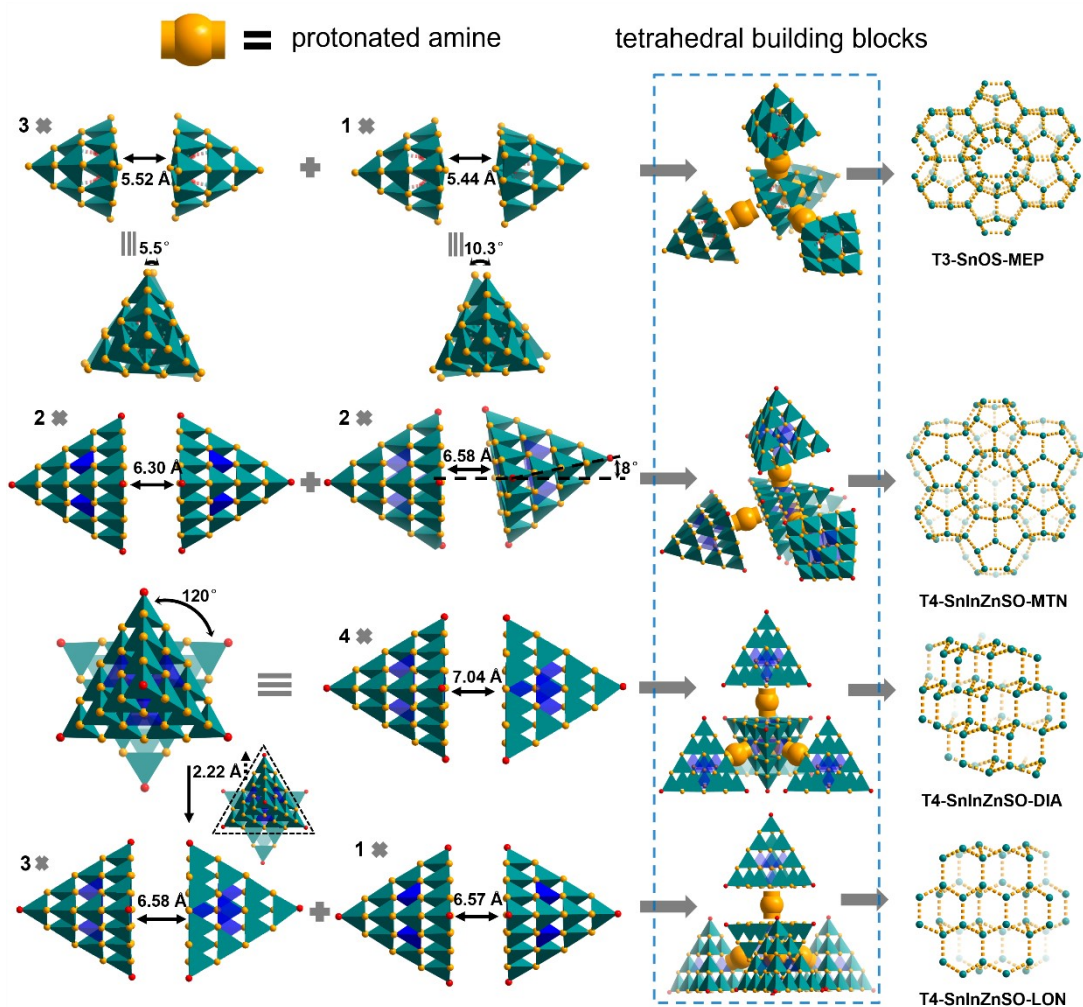
Fig. S7 The different spatial arrangements between Tn clusters for assembling various topologies via coulombic interactions with the protonated organic amine templates.
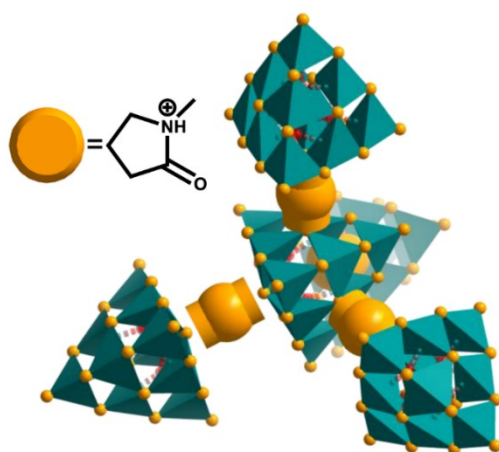
Fig. S8 The linkage mode between oxido-filled-T3 {$Sn_{10}O_4S_{20}$} clusters, each of which connects to four neighbors via the Coulombic interactions with the protonated organic amine templates of H^+NMP.
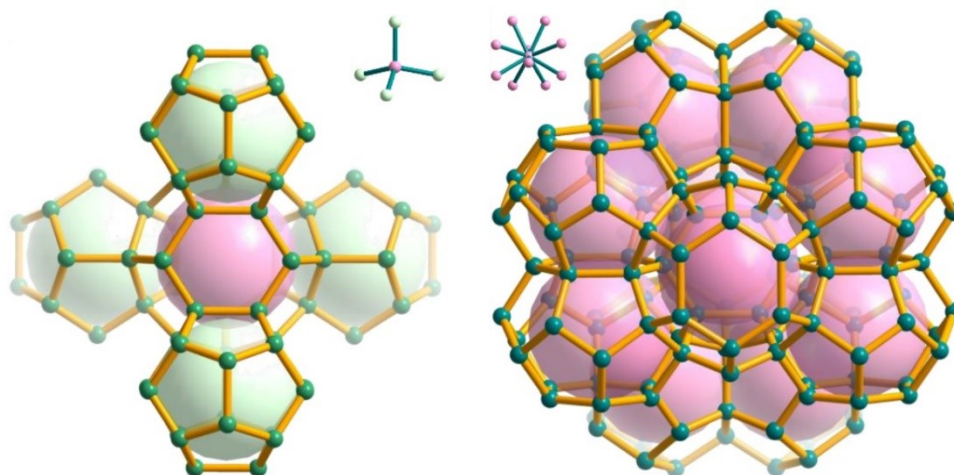
Fig. S9 Each cage-A ($6^2 5^{12}$) surrounded by 4 cage-B (5^{12}) and 10 cage-A ($6^2 5^{12}$) in T3-MEP.
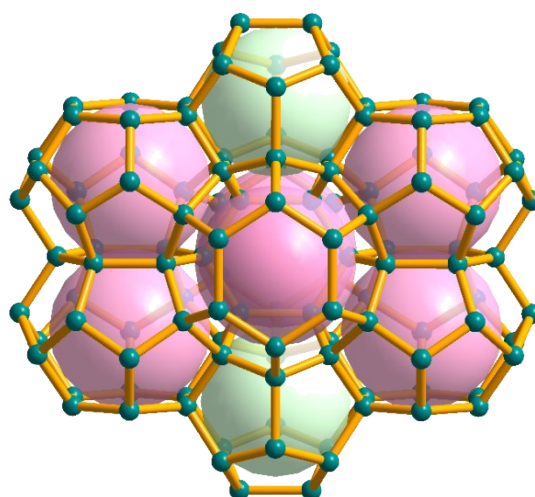
Fig. S10 The $\{Sn_{10}O_4S_{20}\}^{8-}$ anions are scattered in 3D space in an MEP zeotype in which each cluster is treated as a node.
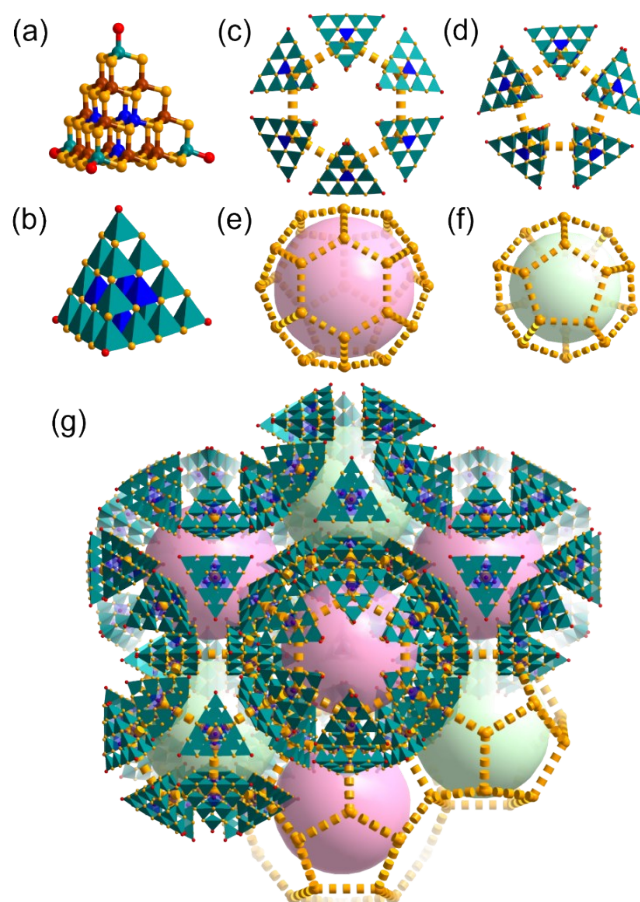
Fig. S11 The crystal structure of T4-MTN (a,b) Discrete supertetrahedral T4-$[Sn_4In_{12}Zn_4O_4S_{31}]^{10-}$. (c) hexagonal and (d) Pentagonal windows. (e) $6^4 5^{12}$ cage-A and (f) 5^{12} cage-B of topological representation. (g) MTN arrangement of T4 cluster anions and its simplified net. Sn, teal; In, brown; Zn, blue; S, gold; O, red.
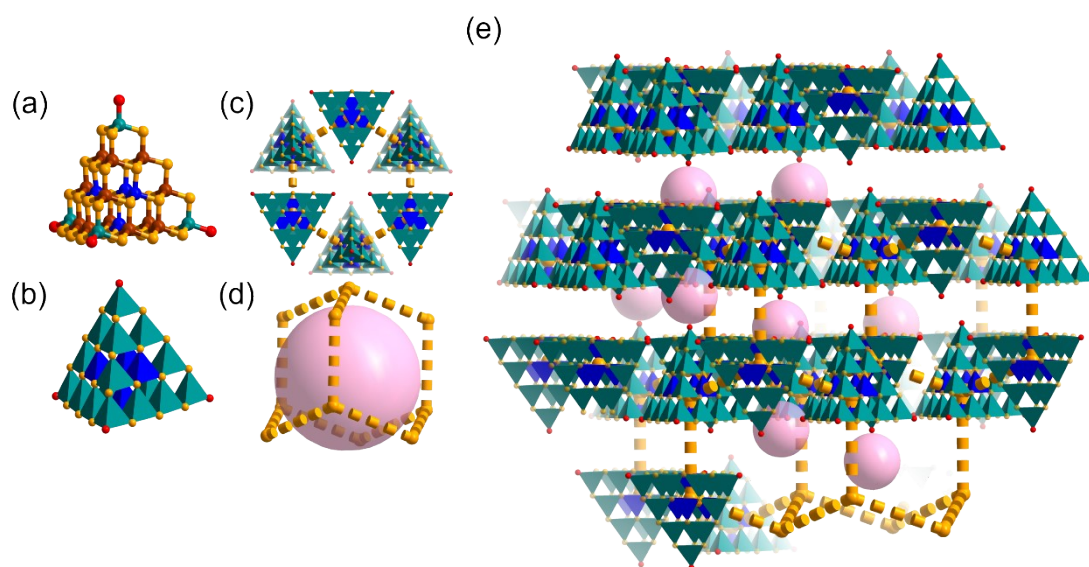
Fig. S12 The crystal structure of T4-DIA. (a,b) Discrete supertetrahedral T4-$[Sn_4In_{12}Zn_4O_4S_{31}]^{10-}$. (c) chair hexagonal windows. (d) 6^4 cage of topological representation. (g) diamond arrangement of T4 cluster anions and its simplified net. Sn, teal; In, brown; Zn,

blue; S, gold; O, red.
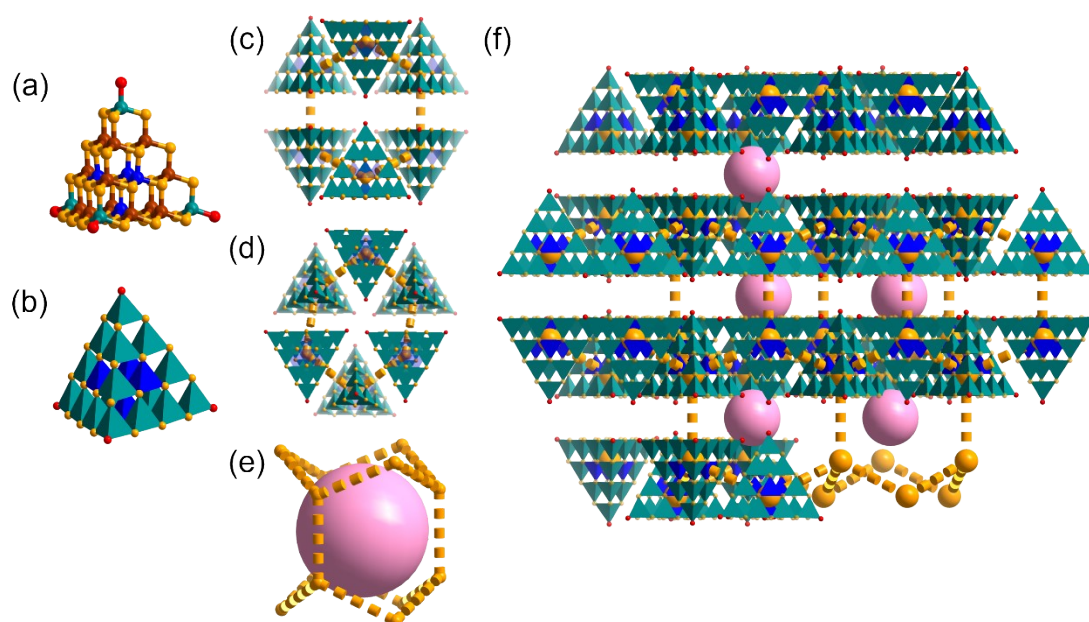
Fig. S13 The crystal structure of T4-LON (a,b) Discrete supertetrahedral T4-$[Sn_4In_{12}Zn_4O_4S_{31}]^{10-}$. (c) boat and chair (d) hexagonal windows. (d) 6^5 cage of topological representation. (g) lonsdaleite arrangement of T4 cluster anions and its simplified net. Sn, teal; In, brown; Zn, blue; S, gold; O, red.
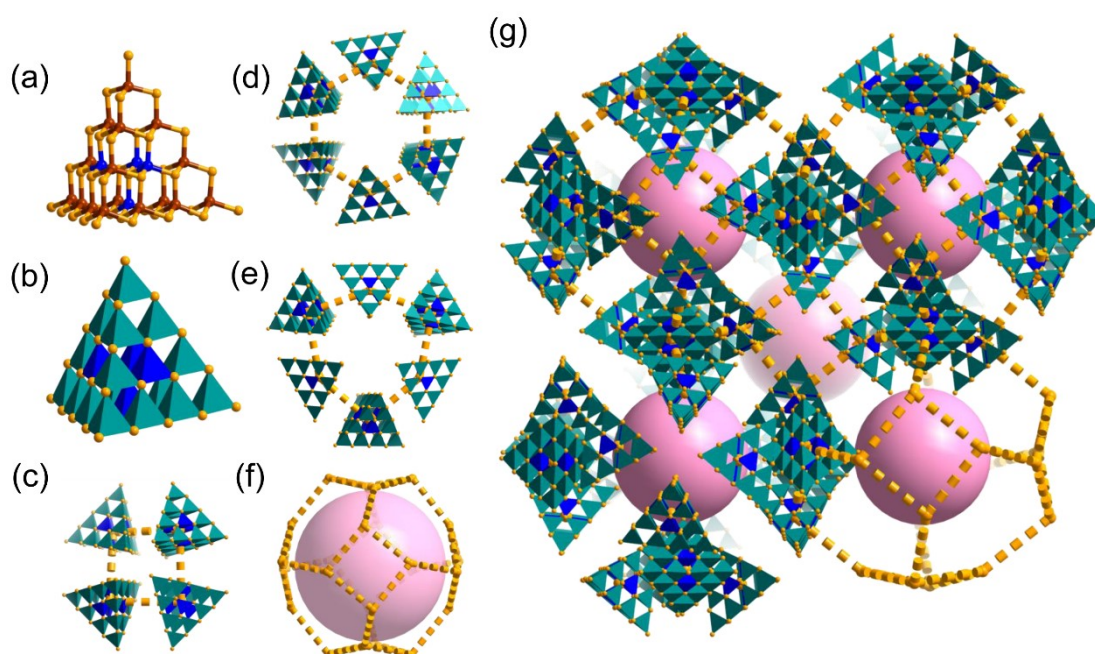
Fig. S14 The crystal structure of T4-SOD (a,b) Discrete supertetrahedral T4-$[In_{16}Zn_4S_{35}]^{14-}$. (c) four-membered (b) six-membered and (e) distorted six-membered ring of window (d) truncated octahedral cage of topological representation. (g) sodalite arrangement of T4 cluster anions and its simplified net. In, brown; Zn, blue; S, gold.

Section S5: Powder X-Ray Diffraction (PXRD)
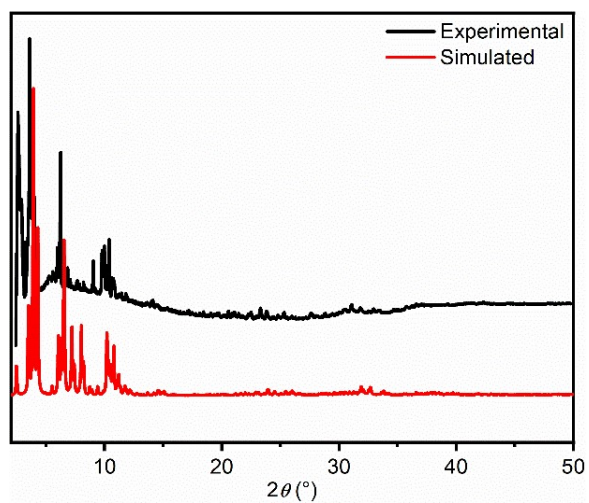
Fig. S15 Experimental and simulated PXRD patterns of T3-MEP.
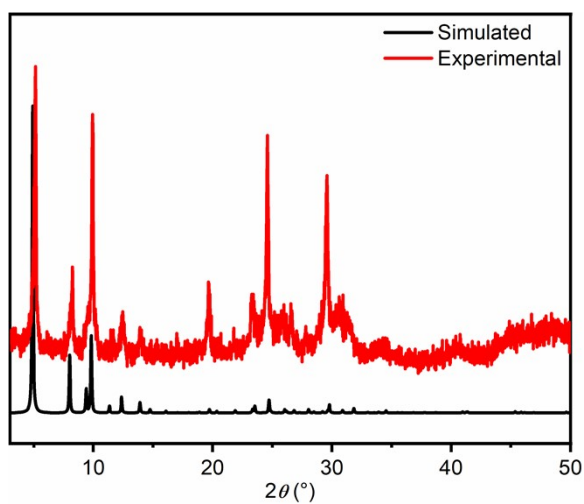
Fig. S16 Experimental and simulated PXRD patterns of T4-DIA.
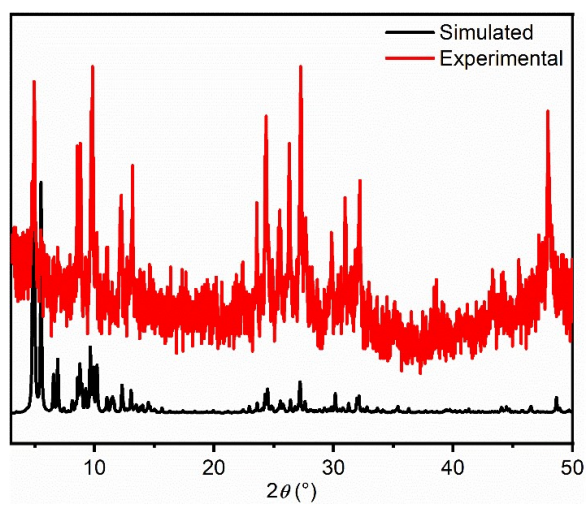
Fig. S17 Experimental and simulated PXRD patterns of T4-LON.
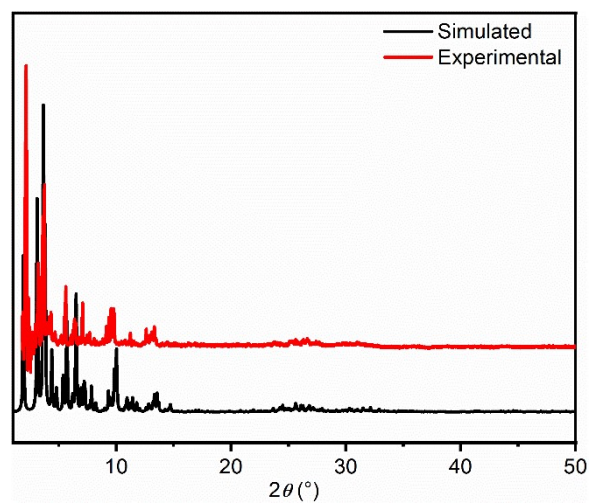
Fig. S18 Experimental and simulated PXRD patterns of T4-MTN.

Section S6: Fourier-Transform Infrared (FT–IR) Spectroscopy
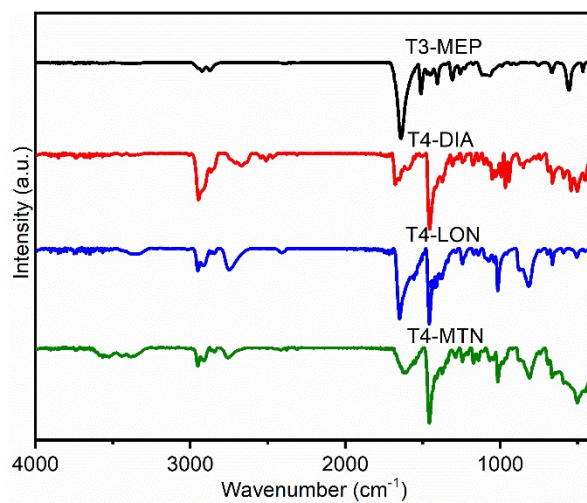
Fig. S19 The FT–IR spectra of samples.

Section S7: Thermogravimetric Analysis (TGA)
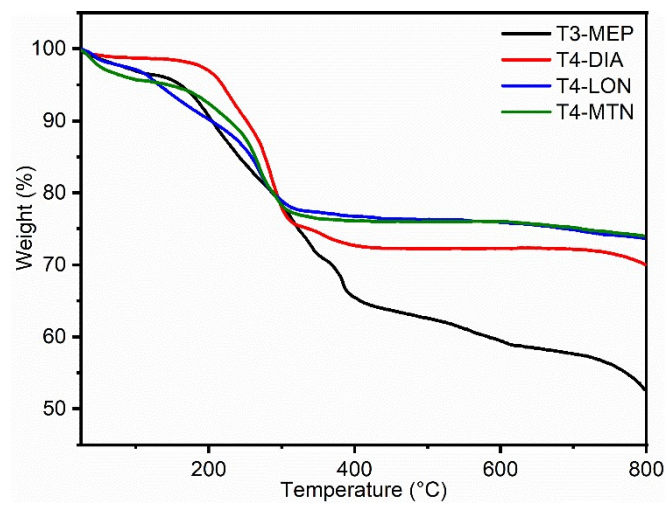
Fig. S20 The TGA curves of samples.

Section S8: Tauc Plots from Ultraviolet Visible (UV–Vis) Diffuse

Reflection Spectroscopy (DRS)
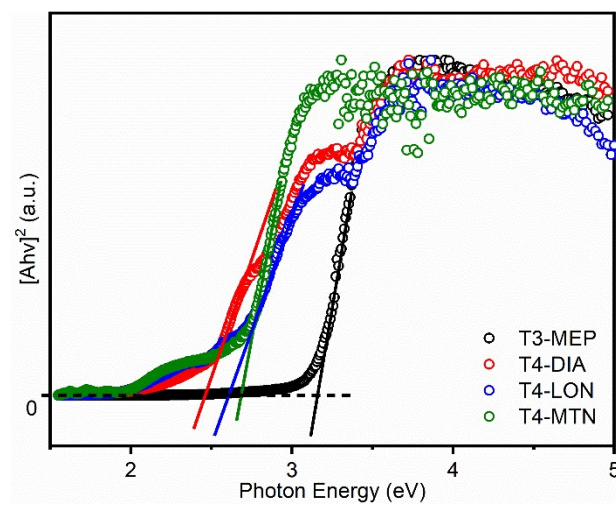
Fig. S21 The tauc plots of samples.

Section S9: Scanning Electron Microscopy (SEM) and X-ray Energy

Dispersive Spectroscopy (EDS)
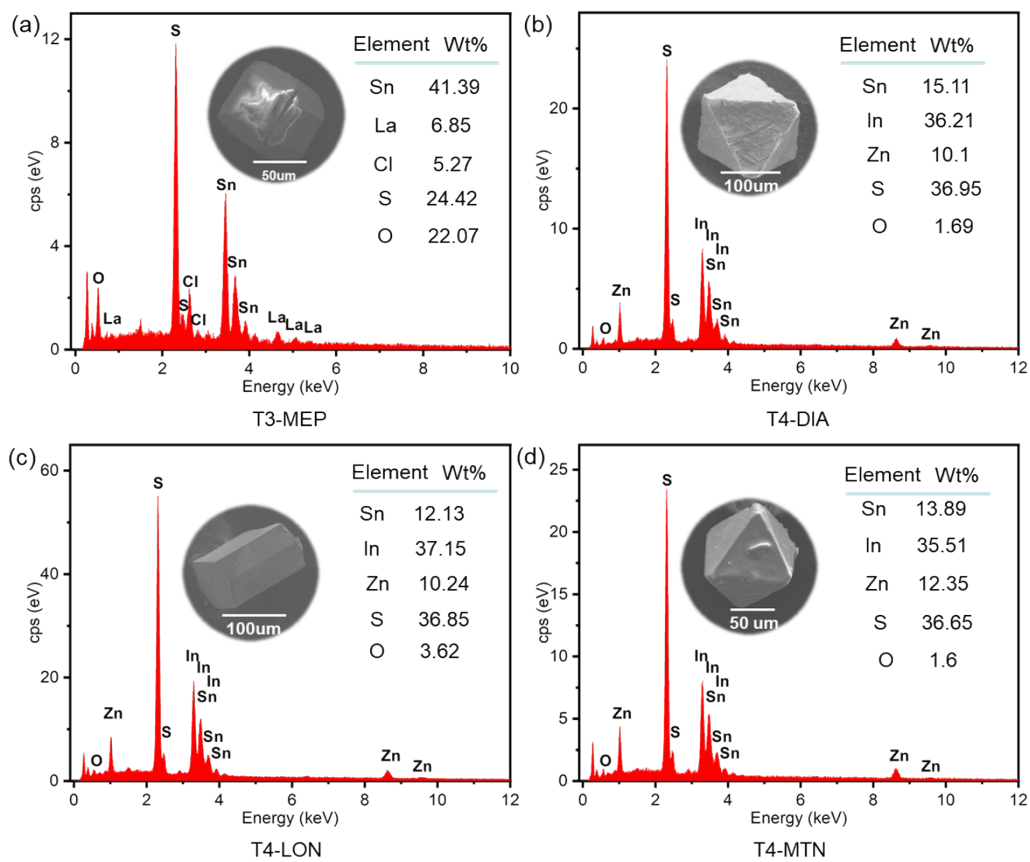
Fig. S22 The SEM images and EDS spectra of samples.

Section S10: Proton Conduction
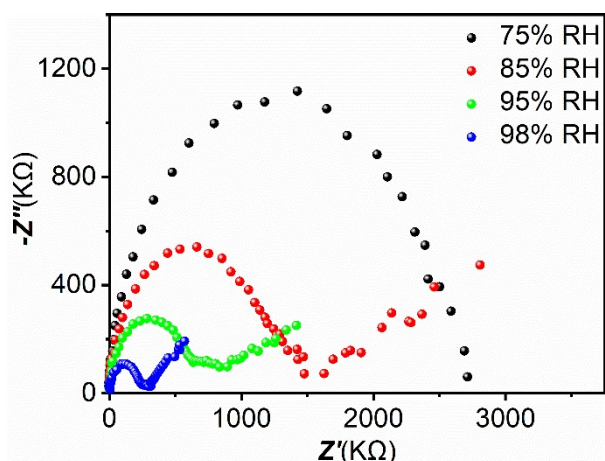
Fig. S23 Nyquist plots of T4-DIA at different RH at 25 °C.
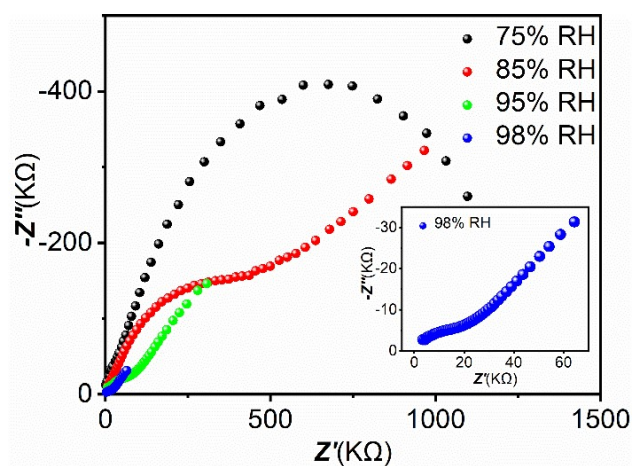
Fig. S24 Nyquist plots of T4-LON at different RH at 25 °C.
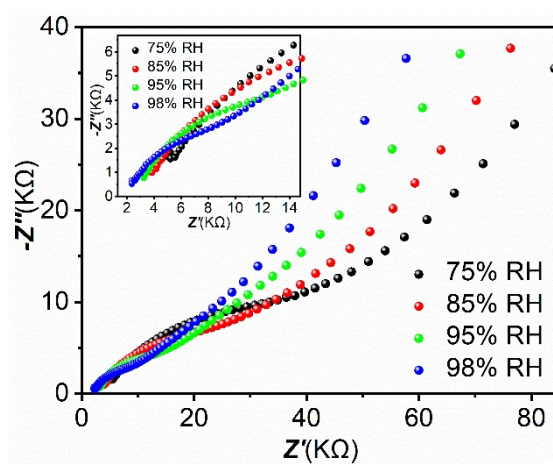
Fig. S25 Nyquist plots of T4-MTN at different RH at 25 °C.
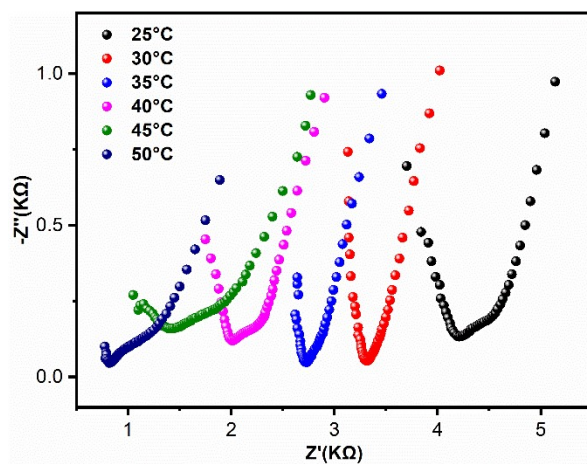
Fig. S26 Nyquist plots of T3-MEP at different temperatures under 98% RH.
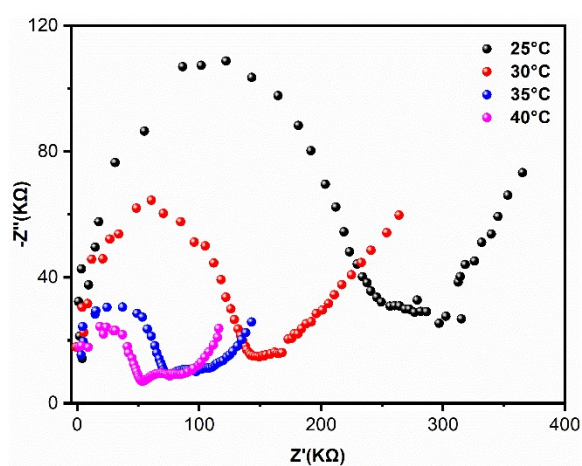
Fig. S27 Nyquist plots of T4-DIA at different temperatures under 98% RH.
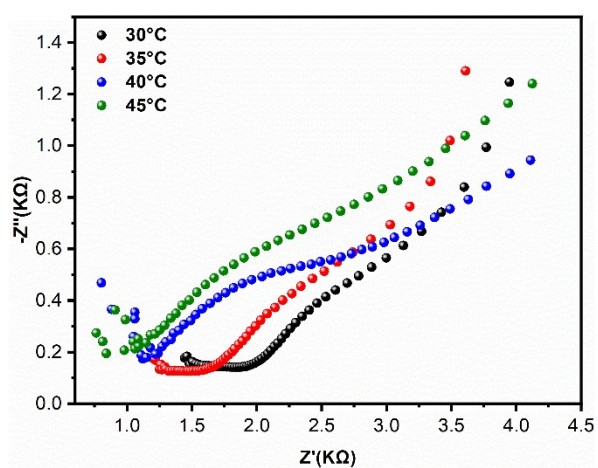
Fig. S28 Nyquist plots of T4-LON at different temperatures under 98% RH.
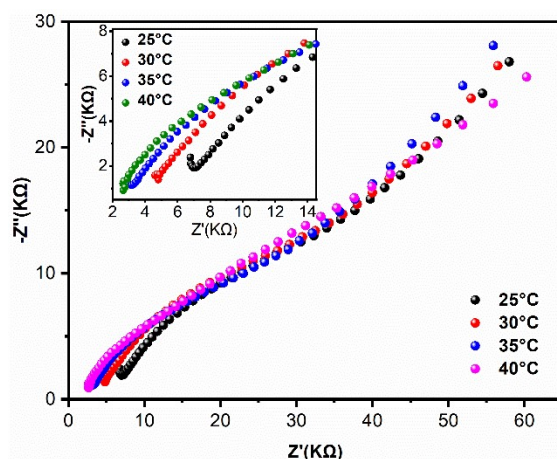
Fig. S29 Nyquist plots of T4-MTN at different temperatures under 75% RH.
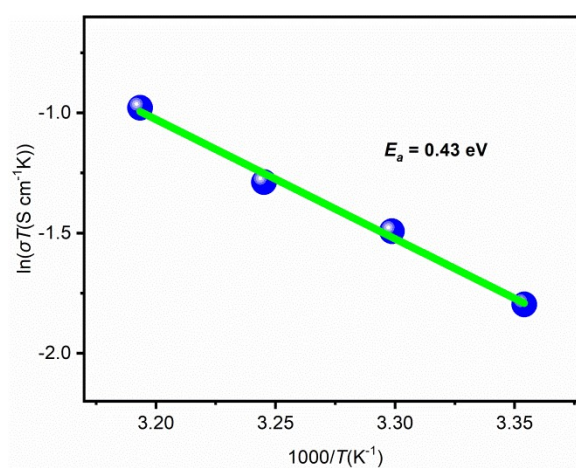
Fig. S30 Arrhenius plots of proton conductivity on the temperature of T4-DIA under 98% RH.
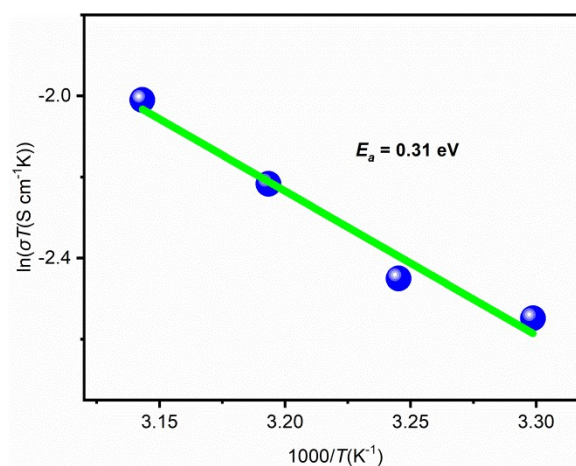
Fig. S31 Arrhenius plots of proton conductivity on the temperature of T4-LON under 98% RH.
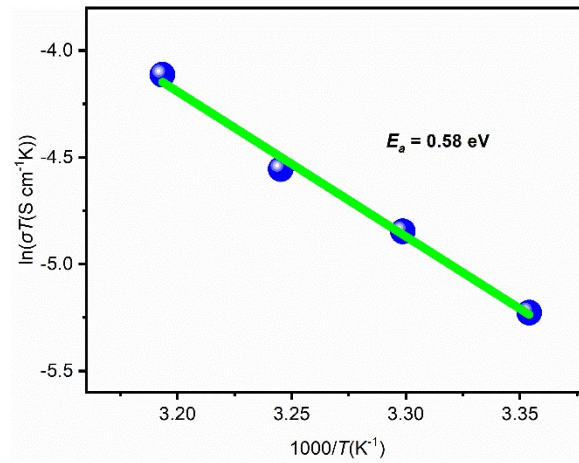
Fig. S32 Arrhenius plots of proton conductivity on the temperature of T4-MTN under 75% RH.

Section S11: References

1 (a) O. V. Dolomanov, L. J. Bourhis, R. J. Gildea, J. A. K. Howard and H. Puschmann, *J. Appl. Cryst*, 2009, **42**, 339-341; (b) G. Sheldrick, *Acta Cryst*, 2015, **C71**, 3-8; (c) L. J. Bourhis, O. V. Dolomanov, R. J. Gildea, J. A. K. Howard and H. Puschmann, *Acta Cryst*, 2015, **A71**, 59-75.

2 P. van der Sluis and A. L. Spek, *Acta Cryst*, 1990, **A46**, 194-201.